JOURNAL OF Materials CHEMISTRY

Relative stabilities, bulk moduli and electronic structure properties of different ultra-hard materials investigated within the local spin density functional approximation

Maurizio Mattesini,* Samir F. Matar, Anders Snis, Jean Etourneau and Alexander Mavromaras

Institut de Chimie de la Matière Condensée de Bordeaux, I.C.M.C.B-CNRS 87, Avenue du Dr. Albert Schweitzer, F-33608 Pessac Cedex, France.
E-mail: maurizio@icmcb.u-bordeaux.fr

Received 17th June 1999, Accepted 17th September 1999

The relative stabilities of the following phases: graphite-C_3N_4, α-C_3N_4, β-C_3N_4, cubic-C_3N_4 and pseudo-cubic-C_3N_4 have been determined using density functional theory in its local density approximation. In particular three calculational methods were imployed: augmented spherical wave, linear muffin-tin orbitals and full-potential linearized augmented plane-wave. The main objective of this work was the prediction of the hardness for a series of C_3N_4 phases (α, β, cubic and pseudo-cubic) as well as for the cubic BN (c-BN) structure. To this purpose total energy calculations were performed for different unit cell volumes and the resulting data were fitted to a polynomial function in order to determine the equilibrium lattice constants (a_{eq} and c_{eq}), bulk moduli (B_0) and pressure derivatives (B_0'). Even though the different methods do not produce comparable energy trends, all methods are in agreement in predicting equilibrium volume, bulk modulus and pressure derivatives. Further, for the graphite-based structures the influence of hybridisation on the chemical bonding and stability is discussed in terms of the site projected densities of states as well as the crystal orbital overlap population. For the hexagonal and orthorhombic phases the electronic properties are also discussed by means of a density of states analysis.

1 Introduction

Superhard materials such as diamond and cubic boron nitride exhibit excellent mechanical, chemical and physical properties. However, it is well known that diamond, for example, cannot be used in cutting tools for steel, owing to its instability at high temperature. For this reason and because of the need to substitute expensive diamond in many other applications, new hard materials are required.

By using an empirical formula which relates the bulk modulus of tetrahedrally coordinated systems to the length and ionicity of their bonds, Cohen predicted in 1985 that a material made from carbon and nitrogen should exhibit a bulk modulus higher than that of diamond owing to the short length and higher covalency of the C–N bond.[1,2] As a consequence, carbon nitrides have been proposed as candidates for new superhard materials. Recently, first principles calculations within the local density approximation (LDA) on the cubic form of C_3N_4 have shown a bulk modulus exceeding that of diamond.[3,4] This phase referred to as cubic-C_3N_4, possesses a predicted bulk modulus of 496 GPa and could be synthesised at high pressure. The investigation of new ultra-hard materials could be based on simple considerations such as electron counting in order to find materials with *isoelectronic* structures (*i.e.* BN is electronically equivalent to two carbons). Consequently a series of different combinations of C, B and N can be investigated for the search of new hard compounds, providing that the following simple condition is respected:

$$pZ_V(B)+mZ_V(C)+lZ_V(N)=4n$$

The values p, m, l and n are integers and $Z_V(B)$, $Z_V(C)$ and $Z_V(N)$ are the atomic valence states (2s and 2p) for boron, carbon and nitrogen, respectively. Examples are represented by the systems C_3N_4, $C_{11}N_4$, BN and BC_2N.

Our goal is to employ a fast and reasonably accurate calculation scheme in order to describe the stability and hardness of carbonitride compounds. For this purpose we compare the output of the usually very accurate full potential approach with two methods based on a spherical shape approximation of the LDA potential. Here, we have focused our attention on the simple C_3N_4 system and as a starting point we have studied the relative stabilities of five hypothetical phases in the C_3N_4 system (graphite-like, α, β, cubic and pseudo-cubic) by using three different density functional theory (DFT) based methods within the LDA:[5] augmented spherical wave (ASW),[6] linear muffin-tin orbitals (LMTO)[7] and full-potential linearized augmented plane-wave (FP-LAPW).[8] For the exchange and correlation effects the parametrisation scheme of Van Barth and Hedin[9] and Janak[10] was used in the ASW and LMTO method, meanwhile in the FP-LAPW the Perdew and Wang 92[11] functional was assumed.

The main purpose of this work is to investigate the hardness of these carbonitrides with different DFT methods by evaluating the compressibility of the systems. Since diamond and cubic boron nitride (c-BN) are the hardest materials known and because their compressibility is well characterised from the experimental point of view, these two systems have also been investigated in order to allow for comparison between theoretical and experimental hardness. Calculations were performed by using the three previously mentioned DFT-based methods to evaluate the total energy of diamond, cubic boron nitride and five different C_3N_4 phases as a function of different unit cell volumes. Data were fitted with a third-order Birch equation to determine the equilibrium volumes, bulk moduli and pressure derivatives. The compressibility and energy of each carbon nitride phase with composition C_3N_4 were then compared.

Further, particular attention has been given to the understanding of the chemical bonding implied in the three different

stacking orders (AAA, ABA and ABC) of the defect graphite-like phase. Finally, the differences in the electronic properties of the hexagonal and orthorhombic graphitic phase are illustrated from the density of states (DOS) plots.

2 Methods and computational details

The total energy of the C_3N_4 system was evaluated within the LMTO and ASW calculations using the tetrahedron method for the k-space integration and 217 irreducible k-points (energy converging with k-points, $\Delta E < 1$ MRyd; 1 Ryd = 13.605698 eV) generated from a uniform $12 \times 12 \times 12$ mesh according to the Monkhorst–Pack[12] scheme. In both methods the atomic sphere approximation (ASA) is used, in which each atom is represented by a sphere. Inside the spheres the potential and charge density are assumed to be spherically symmetric. Then the sum of all sphere volumes is made to equal the volume of the unit cell. Within the ASA one usually has to introduce pseudo-atoms (with atomic number $Z = 0$) or empty spheres in order to ensure a continuous electronic density in open structures. In the present calculations we paid particular attention to an optimal choice of the atomic radii as well as the number and position of empty spheres used to meet the ASA criteria.

For the diamond and c-BN phase a $12 \times 12 \times 12$ mesh was found to ensure the desired convergence.

The full potential total energy calculations of the C_3N_4 phases were performed using the same plane wave cut-off (87 plane waves per atom) and k-point number (300 k-points), as they were optimised for the α-C_3N_4 structure, a phase with the largest number of atoms per unit cell (28). For carbon and nitrogen atom types the same muffin-tin radius ($R_{MT} = 1.33$ Å) was used and maintained fixed for all the investigated C_3N_4 structures.

By using different basis set cut-offs we also found that at the equilibrium volume approximately 87 wave functions per atom were sufficient to predict the bulk modulus for the carbon nitride phases, without any significant change when increasing the number of basis functions used.

For the c-BN system the FP-LAPW calculation was performed in order to estimate the bulk modulus by using the same parameter as Park, Terakura and Hamada.[13]

3 Structures

The geometries of the C_3N_4 phases were taken from the theoretical work of Teter and Hemley,[3] in which the equilibrium structures were determined with a pseudo-potential plane wave approach (PSP).[14]

The hexagonal beta phase (β-C_3N_4) contains 14 atoms per unit cell ($P3$ space group) and consists of four-fold coordinated carbon and three-fold coordinated nitrogen atoms (Fig. 1). This phase is a network of three-, four- and six-fold rings of CN_4 tetrahedra.

The alpha phase (α-C_3N_4) has hexagonal symmetry and contains 28 atoms per unit cell ($P3_1c$ space group). It can be viewed as a sequence of A and B layers in an ABAB stacking in which A is the β-C_3N_4 unit cell and B the mirror image of A (Fig. 2).

The cubic structure (c-C_3N_4) is based on the high-pressure willemite-II structure of Zn_2SiO_4, where C substitutes Zn and Si and N substitutes O. This phase contains 7 atoms per unit cell and belongs to the $I\bar{4}3d$ space group (Fig. 3).

The pseudo-cubic structure, usually called defect-zinc blende structure (bl-C_3N_4), exhibits $P\bar{4}2m$ symmetry and contains 7 atoms per unit cell (Fig. 4).

The graphitic form of C_3N_4 (g-C_3N_4) is represented by a planar structure with an ABA[3] stacking mode (Fig. 5). The hexagonal unit cell contains 14 atoms and the symmetry is

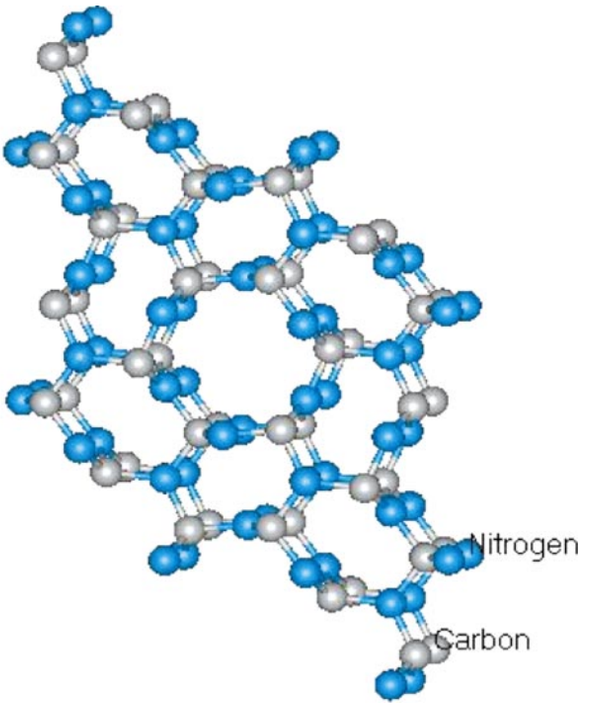

Fig. 1 β-C_3N_4 phase. The carbon and nitrogen atoms are depicted as gray and blue spheres, respectively. This colour scheme is retained in the following figures.

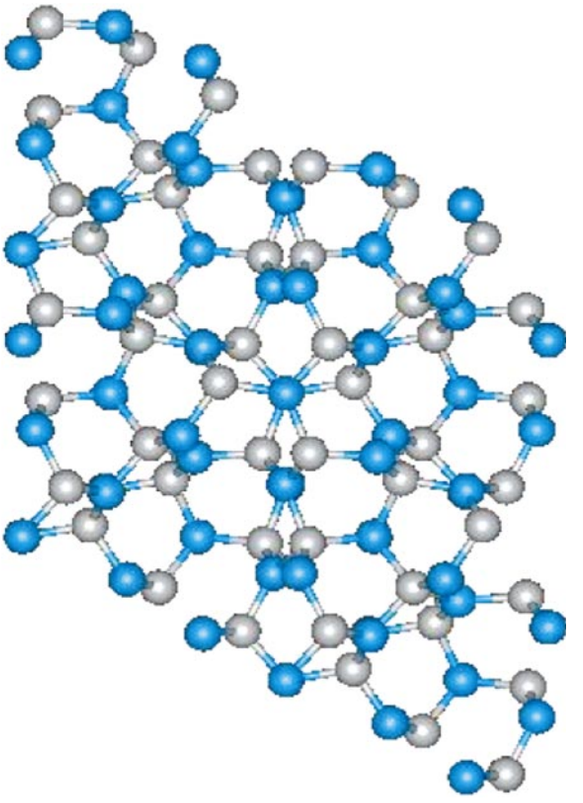

Fig. 2 α-C_3N_4 phase.

$P\bar{6}m2$. Each C atom is three-fold coordinated as is one of the four N atoms per cell. The other three N atoms are two-fold coordinated ('resonating' bonds). This phase has been taken as a reference for the graphite-based structure in making comparison between the relative stabilities of different carbon nitride phases.

For the graphite phase four other forms have been predicted in earlier work. The first (AAA stacking mode[15]) has 7 atoms

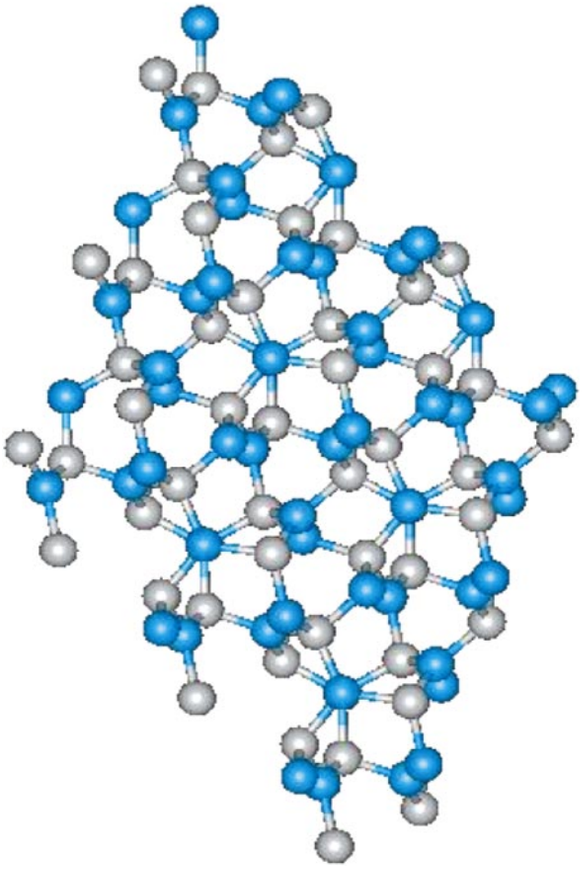

Fig. 3 c-C_3N_4 phase.

per unit cell and the space group is $P\bar{6}m2$. The second phase (ABC stacking mode[16]) which belongs to the $R3m$ space group, shows 7 atoms in the unit cell and consists of graphite-like sheets with ABC rhombohedral stacking order.

The other two phases, recently suggested by Alves *et al.*, [17] are represented by an orthorhombic unit cell (Fig. 6) instead of a hexagonal one (Fig. 7). For this new phase a different vacancy ordering inside the graphitic plane was found. Two new structures ($P2mm$ space group) with respectively AAA (7 atoms per unit cell) and ABA (14 atoms per unit cell) stacking mode were proposed.

In the diamond-like cubic structure of boron nitride (c-BN)[18] two atoms per unit cell are present and the space group is $F\bar{4}3m$. The structure is made of cubic close-packed layers of boron and nitrogen where the atoms are tetrahedrally coordinated (sp^3) and the B–N bonds are strongly covalent.

For diamond lattice geometries were taken from experiment.[19]

4 Relative stabilities of the C_3N_4 phases

For the C_3N_4 system our full potential method predicts the same energy trend found by Teter and Hemley[3] in their pseudopotential plane-wave calculations. While the graphitic form [C_3N_4-g(ABA)] is the most stable one the α phase lies only marginally higher in energy (0.036 eV). The energy of the β phase is found to be 0.615 eV above that of the α structure. Even though the calculated energy difference between graphite and the α phase (0.036 eV) is of the same order of magnitude as that calculated by Teter and Hemley[3] (0.041 eV), the energy difference between the α and β phases is estimated to be 0.615 eV instead of 0.266 eV.[3] Finally the two cubic structures, simple cubic and zinc blende phase, are estimated to have the highest total energy. The simple cubic phase lies at 1.414 eV above the β phase, while the zinc blende lies at 1.617 eV higher.

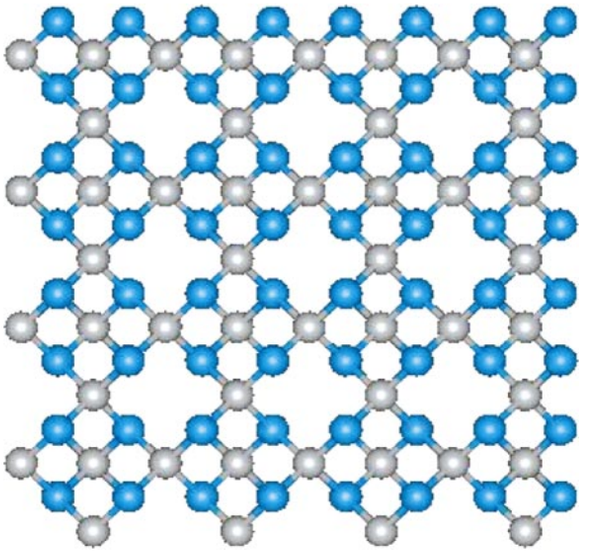

Fig. 4 bl-C_3N_4 phase.

The energy difference found for β-cubic is 1.414 eV instead of 1.015 eV as calculated with the PSP method.[3] In the same way the β-zinc blende energy difference is estimated to be 1.617 eV instead of 1.178 eV.[3]

The use of Liu and Wentzcovitch geometries for the β-C_3N_4 and bl-C_3N_4 phase[16] gives slightly different values for the total energy, but they still confirm the PSP energy trend. The β-phase now lies slightly higher in energy (+0.0215 eV) and the pseudo-cubic slightly lower (−0.038 eV) with respect to our previous calculation (Teter and Hemley geometries[3]).

By contrast, the LMTO and ASW methods predict lower energies for both cubic structures and a higher one for the graphite-like phase. The obtained energy trend follows exactly the atomic densities, indicating that in less compact structures (*i.e.* graphite-like) the ASA approximation is no longer

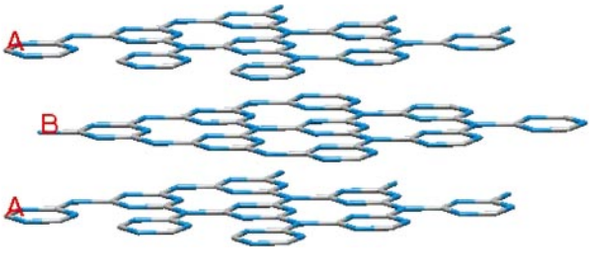

Fig. 5 ABA stacking order in hexagonal C_3N_4 graphitic phase.

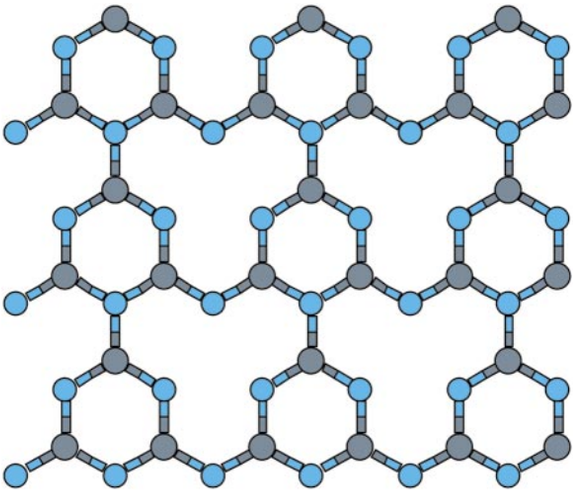

Fig. 6 Orthorhombic structure for the C_3N_4 graphitic phase.

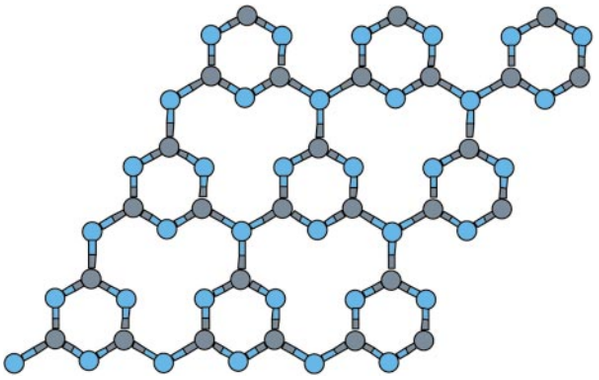

Fig. 7 Hexagonal structure for the C_3N_4 graphitic phase.

acceptable. As a matter of fact, the layered phase is the least dense, the most compressible and it lies at high energy, while the cubic phase is the most dense and least compressible and consequently is predicted to have the lowest energy. Hence, the relative stability trends observed with LMTO and ASW are not comparable with those deduced from FP-LAPW and PSP. This is due to the difficulty of getting reliable results from the use of empty spheres in describing phases with very different atomic packing. For the graphite phase a large amount of empty space must be filled in the unit cell whereas the reverse situation is true for the cubic structure where the ASA worked best.

Even if we cannot make a strict comparison between the relative stabilities, it is important to note that all these DFT methods are in agreement in predicting equilibrium volumes, bulk moduli and their pressure derivatives for c-BN and for all the different phases in the C_3N_4 system (see section 5.1).

5 Hardness

The bulk modulus, $B(V)$, defines the resistance of the material with respect to elastic and isotropic compression. It is related to the curvature of $E(V)$,

$$B(V) = -V\,\frac{\mathrm{d}P}{\mathrm{d}V} = V\,\frac{\mathrm{d}^2E}{\mathrm{d}V^2}$$

where V is the volume of the unit cell, $E(V)$ is the energy per unit cell at volume V, and $P(V)$ is the pressure required to keep the unit cell at volume V. Since the calculations can only provide a restricted set of energies $E(V_i)$, the second derivative $\mathrm{d}^2E/\mathrm{d}V^2$ must be approximated. The least squares fit of the curves E *vs.* V has been done using the first three terms of the Birch equation:[20]

$$E(V) = E_0 + \frac{9}{8}\,B_0V_0\left[\left(\frac{V_0}{V}\right)^{2/3} - 1\right]^2 + \frac{9}{16}\,B_0(B_0' - 4)V_0\left[\left(\frac{V_0}{V}\right)^{2/3} - 1\right]^3 + \sum_{n=4}^{N}\gamma_n\left[\left(\frac{V_0}{V}\right)^{2/3} - 1\right]^n \quad (1)$$

where E_0, V_0, B_0 and B_0' are the equilibrium energy volume, bulk modulus and pressure derivatives of the bulk modulus. The γ_n term represents the total contraction terms.[21] The maximum order of the fit is represented by N. The bulk modulus can then be obtained by analytic differentiation of eqn. (1).

For all the analysed systems, the total energy calculations were performed by applying isotropic compression to the unit cell (keeping the c/a ratio constant). Thus, the isotropic bulk modulus has been estimated with different DFT methods for each structure presented in this work. Table 1 shows the results arising from a third-order fitting of the data set $E(V_i)$.

5.1 Results and discussion

As shown in Table 1, in the C_3N_4 system all DFT methods used in order to predict equilibrium volumes and hence lattice constants, are in good agreements with values from the early pseudo-potential calculations (Teter and Hemley[3]). Using ASW for c-C_3N_4 we obtain a lattice constant larger by 1.65%. The FP-LAPW method usually tends to give the lower values for a and c and they are often very similar to those given by the PSP method.

In the c-BN system we get essentially the same behaviour : the estimated equilibrium volumes are similar and the a lattice constant is smallest for the full potential calculations (Fig. 8).

The predicted bulk modulus (B_0) is usually higher for the FP-LAPW method (Table 1), especially in the cubic C_3N_4 phase for which we obtain a value of 518.40 GPa (see Fig. 9 and 10). This value is very high and larger than that calculated for diamond. Employing a basis set of the same size for diamond, our FP-LAPW yields a bulk modulus of 466.12 GPa ($B_0' = 3.60$ and $a_{eq} = 6.67910\ a_0$), to be compared with an experimental value of 442 GPa. While the predicted bulk moduli of other hypothetical materials (α-C_3N_4, β-C_3N_4 and bl-C_3N_4) approach that of diamond (*ca.* 430–450 GPa), the cubic C_3N_4 clearly exceeds it (518.40 GPa). The cubic phase is predicted to be harder than diamond also from ASW (diamond: $B_0 = 439.80$ GPa; cubic-C_3N_4: $B_0 = 451.85$ GPa) and LMTO calculations (diamond: $B_0 = 453.32$ GPa; cubic-C_3N_4: $B_0 = 468.32$ GPa).

It is important to note that all methods predict the cubic phase to be hardest, with a bulk modulus exceeding that of

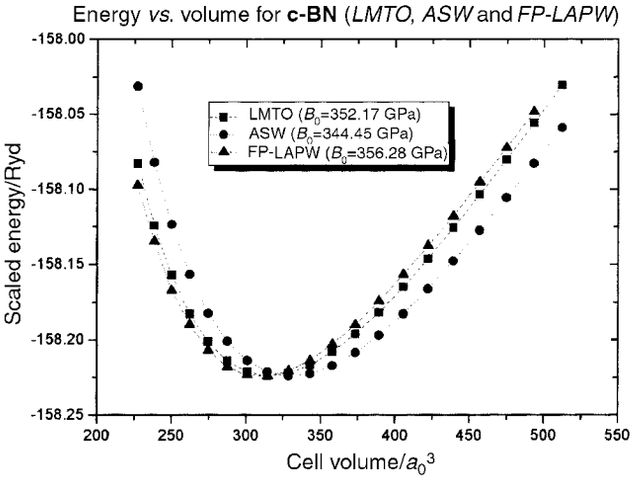

Fig. 8 Energy dependence of the unit cell volume calculated for c-BN with three different DFT methods.

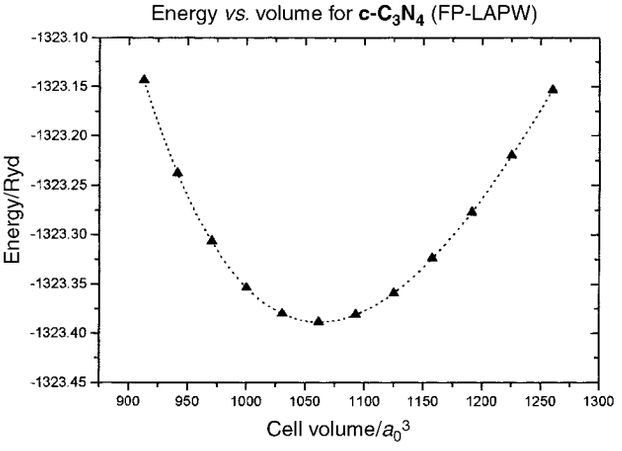

Fig. 9 Total energy dependence *vs.* unit cell volume for c-C_3N_4 with FP-LAPW methods.

Table 1 Equilibrium lattice constants (a_0), bulk modulus B_0 (GPa) and its pressure derivatives, B_0'. The curves E *vs.* volume were fitted with a third-order Birch equation [eqn. (1)]

	β-C_3N_4	α-C_3N_4	c-C_3N_4	bl-C_3N_4	c-BN
$(a_{eq}, c_{eq})_{LMTO}$	$a=12.10040$, $c=4.53808$	$a=12.27410$, $c=8.93561$	$a=10.30175$	$a=6.56200$	$a=6.80743$
$(a_{eq}, c_{eq})_{ASW}$	$a=12.11743$, $c=4.54447$	$a=12.22461$, $c=8.90352$	$a=10.36797$	$a=6.49170$	$a=6.91162$
$(a_{eq}, c_{eq})_{LAPW}$	$a=12.10198$, $c=4.53867$	$a=12.21097$, $c=8.89358$	$a=10.20107$	$a=6.48361$	$a=6.76799$
Ref. 3	$a=12.1135$, $c=4.543$	$a=12.21992$, $c=8.9001$	$a=10.19942$	$a=6.46891$	$a=6.83136$[18]
$B_{0(LMTO)}$	455.27	437.92	468.32	440.75	352.17
$B_{0(ASW)}$	431.25	414.37	451.85	427.13	344.45
$B_{0(LAPW)}$	459.71	431.17	518.40	444.49	356.28
Ref. 3	451	425	496	448	456_{exp},[22] 367[23] 353,[13,24] 362.6[25]
$B_0'_{(LMTO)}$	3.93	3.61	3.98	3.95	3.68
$B_0'_{(ASW)}$	3.61	3.58	3.97	3.89	3.73
$B_0'_{(LAPW)}$	3.33	3.32	4.71	3.64	3.77
Ref. 3	3.3	3.1	3.4	3.4	3.8[18]

diamond, while the α structure is predicted to have the lowest B_0 (highest compressibility).

For the cubic-BN system the bulk moduli are of the same order of magnitude (LMTO: $B_0=352.17$ GPa, ASW: $B_0=344.45$ GPa and FP-LAPW: $B_0=356.28$ GPa) and close to the values given in earlier work (see Table 1). This behaviour fits well into the general picture of ASA methods producing better results for more compact structures (*i.e.* cubic phase). However it should be mentioned that for the cubic-BN system all three methods produce bulk moduli which are *ca.* 100 GPa below the experimental values (Table 1).

The calculated pressure derivatives of the bulk modulus (B_0') for the C_3N_4 system lie between 3 and 4 as shown in Table 1. The FP-LAPW calculation usually gives a better agreement with the reference values (PSP method) except for the cubic phase for which we estimate a surprisingly large value (4.71). All our methods predict, as for the bulk modulus, the highest B_0' for the cubic phase and the lowest one for the α phase, indicating a complete agreement in describing the hardness of these hypothetical C_3N_4 phases.

In the cubic boron nitride structure, B_0' is also well reproduced by all three methods. Like the bulk modulus, the calculated values for B_0' compare well with the results of earlier work and are similar (LMTO: $B_0'=3.68$, ASW: $B_0'=3.73$ and FP-LAPW: $B_0'=3.77$).

6 Chemical bonding in the graphite-like phases

Graphite-like systems consist of 'holey' graphite-like layers with stacking modes AAA (see, for example, Fig. 11), ABA and ABC. Within a layer, carbon atoms form three bonds with neighbouring nitrogen atoms. There are two types of N atoms in the layers, labelled N_{Aro} and N_{Tet} (Fig. 12). Atoms N_{Tet} form three single bonds with neighbouring C atoms, while atoms N_{Aro} form two resonating bonds, one single and one double. The C–N bond lengths inside the layer are approximately of the same order of magnitude in the ABA and ABC phases but they differ slightly from that of the AAA structure (Table 2). In particular, the latter system shows a shorter C–N_{Aro} bond length and a longer C–N_{Tet} bonding. The distances between the sheets in the AAA, ABA and ABC phases are 3.45, 3.36 and 3.07 Å, respectively, and the layers are held together by weak interactions (weak interlayer bonding). Hence the graphite-like structures are not expected to be likely candidates for low compressibility phases but they can represent possible low lying energy systems, *i.e.* thermodynamically more stable.

As previously mentioned, instead of the hexagonal unit cell proposed by Teter and Hemley,[3] a new orthorhombic graphitic form of C_3N_4, resulting from a different order of the carbon vacancies has been proposed by Alves *et al.*[17] (Fig. 6). For this new structure some modifications in the electronic properties are expected owing to a larger electronic participation of the N_{Tet} (nitrogen with three simple N–C bonds) in the C,N-heterocycle. Here a DOS plot has been used to account for whether or not a different order of the vacancies in the graphitic layer might influence the electronic properties.

6.1 Density of states

DOS plots (Fig. 13–15) show that the energy range from −5 eV to E_F is dominated by the N_{Aro} (2s, 2p) states. The main contribution to the Fermi level is thus given in all the three phases by the aromatic nitrogen constituting the C_3N_3 ring (N_{Aro}), while the C dominates the lower part of the valence states (from −10 to −4 eV). At the top of the valence band the AAA phase shows a single broader peak (N_{Aro}) with respect to the other phases owing to the shorter C–N_{Aro} bond length. Moreover the N_{Aro} atom also tends to dominate the lower

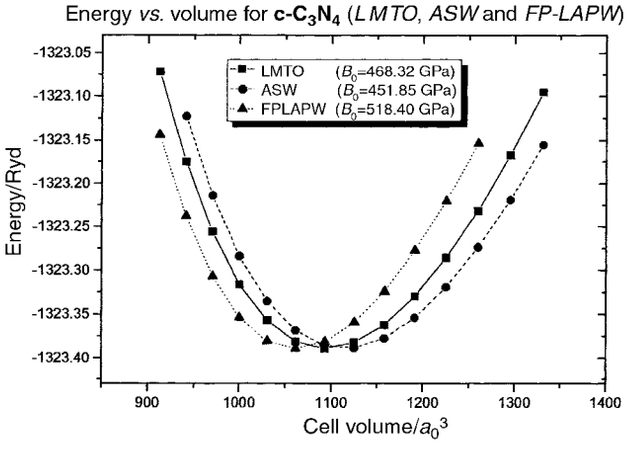

Fig. 10 Energy dependence of the unit cell volume calculated for c-C_3N_4 with three different DFT methods.

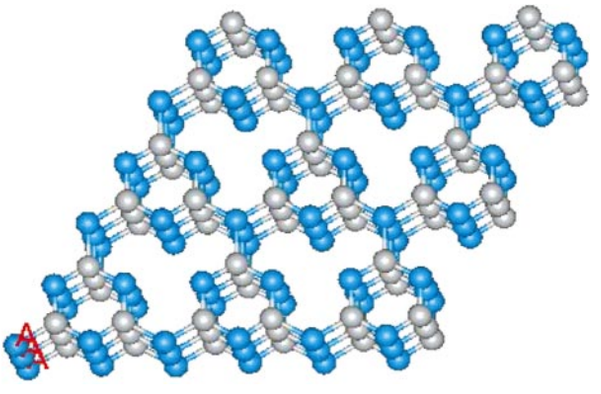

Fig. 11 AAA graphitic phase.

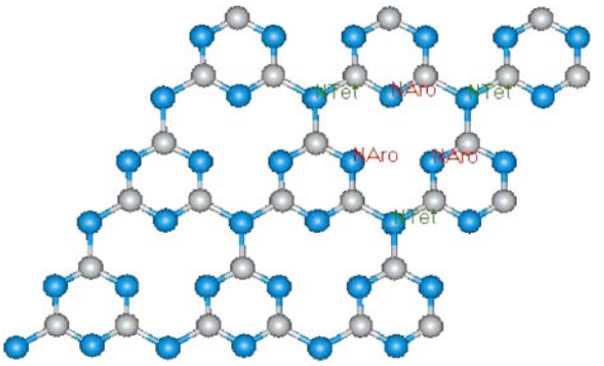

Fig. 12 Two different nitrogens in the graphitic phase: N_{Aro} and N_{Tet}.

energy region of the conduction band (from 1 to 6 eV), while in the ABA and ABC cases the same DOS is found for N_{Aro} and the carbon atom. Around 3 eV (conduction band) all the three phases possess a peak for the N_{Aro} and C states which tends to become higher and narrower by going from the AAA, ABA to the ABC phase. For the AAA structure a DOS for N_{Aro} higher than that of C together with a smoother double peak is found at *ca.* 3 eV. This can also be assigned to the shorter C–N_{Aro} bond inside the C_3N_3 rings and consequently to an increased electron delocalisation inside the heterocycle.

The DOS plot (Fig. 16) for the orthorhombic phase (AAA stacking mode) proposed by Alves *et al.*,[17] clearly shows that a more metallic behaviour is present in this new graphitic form. The electronic levels of the nitrogen atoms belonging to the heterocycle ring and that of the nitrogen with three simple N–C bonds are now crossed by E_F. There is a more significant contribution of electronic states from the N_{Tet} atom close to the Fermi level (compare the same N_{Tet} peak close to the Fermi level in Fig. 13). Generally the nitrogen DOS in the orthorhombic structure is broadened with respect to the DOS of the hexagonal one. This behaviour confirms the assumption of Alves *et al.*[17] about a modification of the electronic structure owing to the stronger role played by N_{Tet} in mediating in between neighbouring heterocycle rings. In contrast to the hexagonal form of graphitic C_3N_4, a semimetallic-like behaviour is thus found in the orthorhombic structure.

6.2 Crystal orbital overlap population

The stabilisation features can be further assessed using chemical bonding criteria. These can be qualitatively discussed by weighting the DOS with the sign and magnitude of the overlap integral between the orbitals of atoms of different sorts. This gives rise to the so-called COOP (crystal orbital overlap population) of which a comprehensive account from the chemistry standpoint has been given by Hoffman.[26] The COOP are positive when they describe bonding states and negative when they describe antibonding states; non-bonding states should exhibit very small intensity COOP. A qualitative description of the chemical bond is given with the recently implemented COOP in the ASW program.[27]

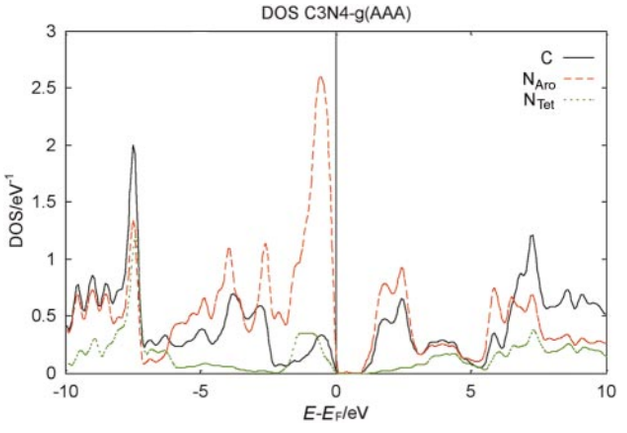

Fig. 13 Site projected DOS for the AAA graphitic phase (ASW method). The energy reference along the *x*-axis is taken with respect to Fermi level (E_F); the *y*-axis gives the DOS per atom and unit energy.

Table 2 Bond distances (Å) in the three different graphite phases. N_{Aro} is the nitrogen belonging to the C_3N_3 ring and N_{Tet} represents the nitrogen atom connecting three C_3N_3 rings inside the layer

Graphitic phase	*d*(C–N_{Aro})	*d*(C–N_{Tet})	*d*(Layers)
AAA	1.2817	1.4861	3.45
ABA	1.3188	1.4484	3.36
ABC	1.3195	1.4435	3.07

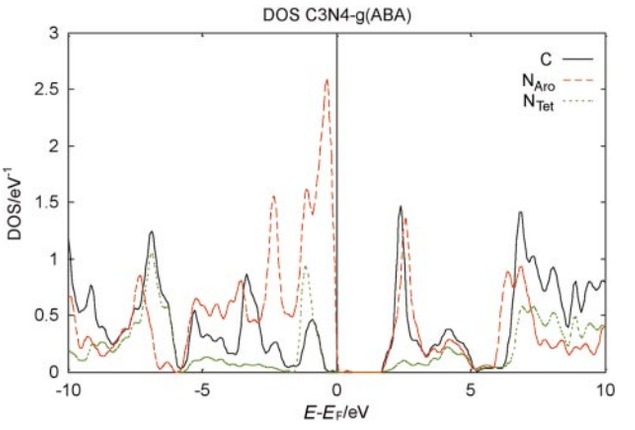

Fig. 14 Site projected DOS for the ABA graphitic phase (ASW method).

The total COOP for the three different graphitic C_3N_4 forms are shown in Fig. 17. In, as far as in all three forms, the interlayer distance ranges from 3.07 Å to 3.45 Å these COOP can be considered to be mainly describing the in-layer interactions between carbon and nitrogen. In the lower energy region of the valence band the three curves are mainly of bonding character but at energies closer to the Fermi level the antibonding states start to dominate. The antibonding counterparts of the conduction band are found centred around 2 and 7 eV while a bonding behaviour appears at higher energy.

From this picture a qualitative explanation of the relative stability implied in the layers of the three graphitic phases can be given by taking into account the intensity of the antibonding states (negative COOP). The fact that a large part of the

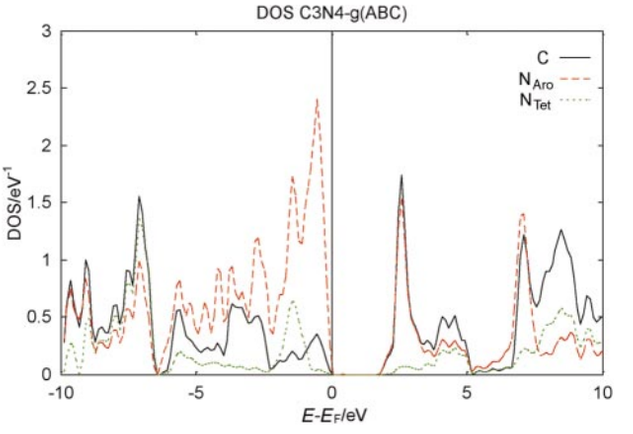

Fig. 15 Site projected DOS for the ABC graphitic phase (ASW method).

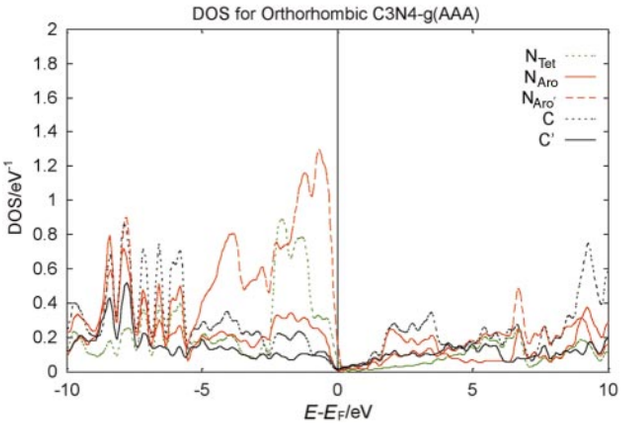

Fig. 16 Site projected DOS plot for the AAA orthorhombic graphitic phase (ASW method).

valence band is principally of bonding character for all the different stacking modes makes the antibonding peak close to the Fermi level (valence band) and those in the conduction band the main discrimination point for accounting different stabilities (see the arrows in Fig. 17). The lower magnitudes of the COOP intensity close to the Fermi energy (valence region) and at about 2 and 7 eV (conduction band) point to a higher stability of the AAA phase with respect to the ABA and ABC. Following this interpretation the bonding network found inside the layers of the AAA phase should bring more stability to the graphitic C_3N_4 system. The ABA and ABC structures should, by contrast, have a comparable stability. This trend is also confirmed by a plot of the integrated COOP (Fig. 18), where the AAA phase can be seen to have the lowest antibonding character in the conduction region.

The stability of the AAA phase with respect to the ABA and ABC can be attributed to shorter $C–N_{Aro}$ bond lengths (Table 2) which implies stronger bonding conditions inside the graphitic layers. This shorter and stronger bonding brings about higher stability and a reduction of the band gap corresponding to a more metallic behaviour.

It should be mentioned that our calculational scheme (*i.e.* relying on the LDA as well as on the ASA) does not reproduce the interplanar interactions which are believed to play an important role in the graphitic compounds.[28] In order to have a complete overview of the relative stability involved in the different packing systems (AAA, ABA and ABC), the strongest bonding interactions found within the sheets of the AAA phase should be weighted with the interatomic potential acting in between the layers (van der Waals potential) in order to achieve a more reliable description of these layered systems.

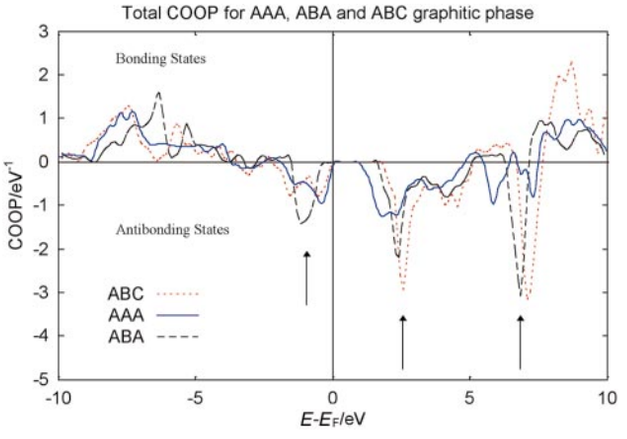

Fig. 17 Total COOP for the three different graphitic phases AAA, ABA and ABC.

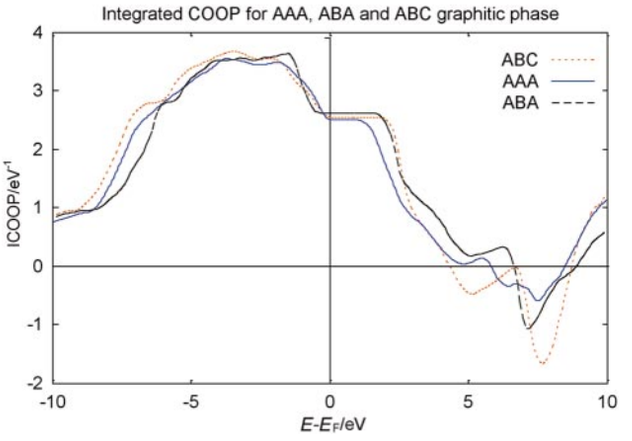

Fig. 18 Integrated COOP for the three different graphitic phases AAA, ABA and ABC.

7 Concluding remarks

Using three different first-principles total energy techniques, we have examined a series of hypothetical C_3N_4 solid phases to determine their total energy and hardness. The use of FP-LAPW method predicts relative energy trends of graphite-, β-, α-, cubic- and pseudo-cubic-C_3N_4 in agreement with the early PSP calculations. The graphitic and α phases are predicted to have the lowest energy with high compressibility, while the two cubic phases are energetically less stable but show higher bulk moduli. These findings are in agreement with the energy trends showed by Liu and Wentzcovitch,[16] provided calculations are carried out using the same geometry. By contrast, the ASA based LMTO and ASW methods cannot reproduce a reasonable energy trend owing to the difficulty of describing, with the same accuracy, phases with different atomic densities. The ASA approximation fits quite well for the cubic structures but not for less compact systems such as, for instance, graphitic phases. Even though we cannot compare the relative stabilities, LMTO and ASW techniques reproduce the lattice constants and especially the bulk moduli in good agreement with the FP-LAPW and PSP methods. As a matter of fact all three methods predict the highest B_0 for the cubic-C_3N_4 phase and the lowest for the α-C_3N_4 phase (Table 1).

It was also found that even if the energy curves $E(V_i)$ obtained from the LMTO, ASW and FP-LAPW methods are slightly shifted with respect to each other along the abscissa axis (volume axis), they tend to show a very similar *curvature*, which determines the hardness of the system. The fact that our bulk moduli and their pressure derivatives are in agreement with each other and compare quite well with the early PSP calculations, demonstrates that all these DFT methods are suitable for describing the hardness of ultrahard materials such as carbon nitrides, even if the trends of the relative stabilities cannot be directly related with each other.

Further, to describe the role of the chemical bonding within the crystal lattice of the graphitic phases, an analysis of the DOS and the COOP was carried out. The DOS analysis for all the three phases clearly shows that, at the top of the valence band, the N_{Aro} atoms have the highest intensity. Because in the same region, and in a large part of the conduction band, the COOP plots show different antibonding magnitudes, we can now qualitatively estimate the relative stabilities of the different phases by looking at the $C–N_{Aro}$ antibonding character. The hexagonal AAA phase is then predicted to have a slightly lower antibonding intensity and hence a higher stability of the layers with respect to the other two phases.

Finally, from a DOS analysis a more metallic behaviour was found for the AAA orthorhombic graphitic phase owing to a stronger participation of the N_{Tet} atoms in the electron delocalisation of the 'C_3N_3' rings.

Acknowledgements

This work was financially supported by the Training and Mobility of Researchers (TMR) Network : *Synthesis, structure and properties of new carbon based hard materials.*

References

1 M. L. Cohen, *Phys. Rev. B: Condens. Matter*, 1985, **32**, 7988.
2 A. Y. Liu and M. L. Cohen, *Science*, 1989, **245**, 841.
3 D. M. Teter and R. J. Hemley, *Science*, 1996, **271**, 53.
4 S. Han and J. Ihm, *Phys. Rev. B: Condens. Matter*, 1997, **55**, 15 349.
5 W. Kohn and L. J. Sham, *Phys. Rev. A: Gen. Phys.*, 1965, **140**, 1133.
6 A. R. Williams, J. Kübler and C. D. Gelatt Jr., *Phys. Rev. B: Condens. Matter*, 1979, **19**, 6094.
7 O. K. Andersen, *Phys. Rev. B: Condens. Matter*, 1975, **12**, 3060; O. K. Andersen and O. Jepsen, *Phys. Rev. Lett.*, 1984, **53**, 2571.
8 P. Blaha, K. Schwarz and J. Luitz, WIEN97, Vienna University of Technology 1997. (Improved and updated UNIX version of the original copyrighted WIEN-code, which was published by P. Blaha, K. Schwarz, P. Sorantin and S. B. Trickey, *Comput. Phys. Commun.*, 1990, **59**, 399).
9 J. Van Barth and D. Hedin, *J. Phys. C*, 1972, **5**, 1629.
10 J. F. Janak, *Solid State Commun.*, 1978, **25**, 53.
11 J. P. Perdew and Y. Wang, *Phys. Rev. B: Condens. Matter*, 1992, **45**, 13 244.
12 H. J. Monkhorst and J. D. Pack, *Phys. Rev. B: Condens. Matter*, 1976, **13**, 5188.
13 K. T. Park, K. Terakura and N. Hamada, *J. Phys. C*, 1987, **20**, 1241.
14 M. C. Payne, M. P. Teter, D. C. Allan, T. A. Arias and J. D. Jannopoulos, *Rev. Mod. Phys.*, 1992, **64**, 1045.
15 J. Ortega and O. K. Sankey, *Phys. Rev. B: Condens. Matter*, 1995, **51**, 2624.
16 A. Y. Liu and R. M. Wentzcovitch, *Phys. Rev. B: Condens. Matter*, 1994, **50**, 10 362.
17 I. Alves, G. Demazeau, B. Tanguy and F. Weill, *Solid State Commun.*, 1999, **109**, 697.
18 L. Vel, G. Demazeau and J. Etourneau, *J. Mater. Sci. Eng. B*, 1991, **10**, 149.
19 C. Kittel, *Introduction to Solid State Physics*, John Wiley & Sons, Inc., New York, 6th edn., 1986 (ISBN 0-471-87474-4).
20 F. Birch, *J. Geophys. Res.*, 1978, **83**, 1257.
21 G. R. Barsch and Z. P. Chang, *J. Appl. Phys.*, 1968, **39**, 3276.
22 J. Sanjurgo, E. Lopez-Cruz, P. Vogl and M. Cardona, *Phys. Rev. B:*, *Condens. Matter*, 1983, **28**, 4579.
23 R. M. Wentzcovitch, K. J. Chang and M. L. Cohen, *Phys. Rev. B: Condens. Matter*, 1986, **34**, 1071.
24 S. Matar, V. Gonnet and G. Demazeau, *J. Phys. I Fr.*, 1994, **4**, 335.
25 P. E. Van Camp, V. E. Van Doren and J. T. Devreese, *Phys. Status Solidi B*, 1988, **146**, 573.
26 R. Hoffmann, *Angew. Chem., Int. Ed. Engl.*, 1987, **26**, 846.
27 V. Eyert, *Electronic structure calculations for crystalline materials*, in *Density Functional Methods: Applications in Chemistry and Materials Science*, ed. M. Springborg, Wiley, Chichester, 1997, pp. 233–304.
28 M. C. Schabel and J. L. Martins, *Phys. Rev. B: Condens. Matter*, 1992, **46**, 7185.

Paper 9/04840E